COUPLING OF THE ANALYTICAL SOLUTION FOR THE TIMOSHENKO BEAM WITH A FULLY SATURATED HALFSPACE BY APPLICATION OF THE WAVE BASED METHOD

M. Lainer and G. Müller

Chair of Structural Mechanics, Technical University of Munich
Arcisstrasse 21, 80333 Munich
e-mail: mirjam.lainer@tum.de, gerhard.mueller@tum.de

Keywords: Wave Based Method, Biot's theory, Soil structure interaction, Timoshenko beam.

Abstract. *To model the field response of a fully saturated halfspace coupled with an elastodynamic trench, the Wave Based Method (WBM) is applied. This numerical method represents an indirect Trefftz approach and is based on weighted wave functions to describe field responses. The wave functions are derived from the analytical solutions for the underlying differential equations. This method has firstly been introduced for vibroacoustic problems in the mid-frequency range. Amongst others, the performance of the WBM strongly depends on the relation between the applied excitation frequency and the dimensions of the observed problem. This relation lies about in the same range for a vibroacoustic structure as for a soil halfspace, which permits to use similar wave function sets. Considering a fully saturated poroelastic halfspace, a second irrotational potential is introduced according to Biot's theory. This so-called second P-wave is approximated by an additional set of wave functions, which increases the number of unknowns for the numerical model. To reduce the total number of wave functions, the coupled trench is modeled by a Timoshenko beam. This permits to replace the wave function sets of the original elastodynamic trench by the analytical solution for the Timoshenko beam. Simulation results are used to assess the accuracy and the mitigation efficiency of the wave barrier.*

1   INTRODUCTION

Open or infilled trenches [1, 2, 3] are often installed to reduce vibrations induced for example by traffic or machinery, which are acting on constructions. Even though pure open trenches are highly effective as wave barriers against incoming Rayleigh waves, their excavation often needs to be stabilized to reach an effective depth. This is especially the case, when the trench is inclined or the surrounding ground is water saturated. To stabilize such an excavation, it is possible to create i.a. a simple wall, an infilled trench with concrete or an open trench with sheet walls. To consider the interaction between such a wave barrier and a water saturated halfspace, different numerical methods have been introduced. One often used approach is to model the wave barrier and the halfspace by the finite element method (FEM) [4, 5]. This usually requires a large amount of degrees of freedom, to model the far field of of the poroelastic halfspace adequately. An alternative presents for example the coupling of the FEM mesh for the wave barrier to a boundary element model (BEM) for the poroelastic halfspace [6].

In this paper, the Wave Based Method (WBM) is extended to model a simple wall as a wave barrier, which is coupled to a poroelastic halfspace. This approach is chosen as the WBM needs less degrees of freedom than a FEM approach. Moreover, the WBM permits to extend such a model by additional inclined soil layers, by introducing compatibility and equilibrium equations between the different soil layers. However, the investigation of different soil layers with the WBM is not analyzed in this paper and is part of future work. The WBM is originally developed by [7] to describe vibro-acoustic problems in the mid-frequency range. It is based on weighted wave functions to approximate the underlying potentials of a boundary value problem. As shown by [7] for an acoustic problem and by [8] for an elastodynamic problem, these wave functions are derived from the underlying analytical solution of a boundary value problem. In further publications, the WBM is extended to model coupled FEM and WBM domains [9, 10] and to treat poroelastic materials according to Biot's theory for higher frequencies [11]. These publications revealed that the WBM shows a high convergence rate and requires significantly less degrees of freedom than a FEM approach. Moreover, [11] gives an example to model coupled poroelastic domains with different material properties by introducing compatibility and equilibrium equations.

These findings motivated to extend the WBM by Biot's theory for low frequencies [12, 13] to model a poroelastic halfspace, coupled to a simple wall. To approximate the Sommerfeld radiation condition, the WBM is extended by an absorbing boundary condition [14], which transmits normally incident wave fronts. The trench wall is modeled by the analytical solution for a Timoshenko beam [15, 16, 17], to consider influences from its shearing behaviour. To couple the deformation field of the Timoshenko beam to a poroelastic halfspace, compatibility and equilibrium conditions are set up and boundary conditions are formulated for the beam. These compatibility and equilibrium equations are involved into a weighted residual Galerkin approach, to derive the final system of linear equations. The defined boundary conditions for the beam are then added to the final system of linear equations, which is solved to derive the unknown weighting values for the wave functions of the WBM domains and the homogeneous solution of the beam. A similar approach is also presented by [7] to couple a Kirchhoff plate to an acoustic cavity.

The paper is organized as follows. In Section 2, Biot's theory for low frequencies is introduced and it is described, how the defined displacement fields for a poroelastic halfspace are approximated by the WBM. Moreover, the analytical solution for the longitudinal and vertical displacement field of a Timoshenko beam are presented and it is shown how these are coupled

to the attached WBM domains. In Section 3, a numerical example is presented to check the convergence of the WBM and to compare the results with data from the publication [6].

2 GOVERNING EQUATIONS AND NUMERICAL MODEL

2.1 Biot's theory for a fully saturated halfspace

The displacement field for a fully saturated halfspace is divided into the solid phase displacements $\mathbf{u}^s = [u_x, u_y]^T$ and the fluid seepage field $\mathbf{U} = [U_x, U_y]^T$. The fluid seepage field describes the relative displacements between the enclosed fluid and the solid skeleton, which is weighted by the porosity n^f: $\mathbf{U} = n^f(\mathbf{u}^f - \mathbf{u}^s)$. These displacement fields are described by a superposition of the gradients of two irrotational potentials $\Phi_{p_{1/2}}$ and the curl of one solenoidal potential Ψ_s, based on Biot's theory [12, 13]. The approximation of these potentials with the Wave Base Method (WBM) is shown in the next subsection.

$$\mathbf{u}^s = \boldsymbol{\nabla}\Phi_{p_1} + \boldsymbol{\nabla}\Phi_{p_2} + \widetilde{\boldsymbol{\nabla}}\Psi_s \tag{1}$$

$$\mathbf{U} = \gamma_{p_1}\boldsymbol{\nabla}\Phi_{p_1} + \gamma_{p_2}\boldsymbol{\nabla}\Phi_{p_2} + \gamma_s\widetilde{\boldsymbol{\nabla}}\Psi_s \tag{2}$$

The values $\gamma_{p_{1/2}}$ and γ_s in equation (2) describe eigenvalues of the two dynamic equations according to Biot's theory for low frequencies [12], when these are solved either for $\boldsymbol{\nabla}\Phi_{p_{1/2}}$ or $\widetilde{\boldsymbol{\nabla}}\Psi_s$. Moreover, these potentials correspond to the so-called first and second P-wave and the S-wave, which are characterized by their wave numbers $k_{p_{1/2}}$ and k_s. These wave numbers are described by the following equation and depend on the radial excitation frequency $\omega = 2\pi f$ as well as on the material parameters summarized in Table 1. Moreover, the wave numbers for the first and second P-wave depend on the parameter ρ_{f2}, which indicates the coupling between fluid phase and solid skeleton. Its imaginary part depends on the dissipation parameter ξ.

$$k_{p_{1/2}} = \sqrt{\frac{\rho_f + \gamma_{p_{1/2}}\rho_{f2}}{(\alpha + \gamma_{p_{1/2}})M}} \cdot \omega, \quad k_s = \sqrt{\left(1 + \gamma_s\frac{\rho_f}{\rho}\right)\frac{\rho}{\mu}} \cdot \omega \tag{3}$$

$$\text{with } \rho_{f2} = \frac{\rho_f a}{n^f} - \frac{\mathrm{i}\xi}{\omega(n^f)^2}, \quad \xi = \frac{\rho_f \cdot (n^f)^2}{k_c} \cdot 9.81\mathrm{m/s}^2, \quad k_c = \frac{\kappa \cdot \rho_f}{\eta_f} \cdot 9.81\mathrm{m/s}^2$$

Based on the description of the displacement fields, given by the equations (1) and (2), the following compatibility equations are defined for a poroelastic halfspace. Here, the value ζ describes the divergence of the fluid seepage field, or respectively the amount of fluid leaving the pores.

$$\begin{pmatrix} \varepsilon_{xx} \\ \varepsilon_{yy} \\ \gamma_{xy} \\ \zeta \end{pmatrix} = \begin{bmatrix} \frac{\partial}{\partial x} & 0 & 0 & 0 \\ 0 & \frac{\partial}{\partial y} & 0 & 0 \\ \frac{\partial}{\partial y} & \frac{\partial}{\partial x} & 0 & 0 \\ 0 & 0 & \frac{\partial}{\partial x} & \frac{\partial}{\partial y} \end{bmatrix} \begin{pmatrix} u_x \\ u_y \\ U_x \\ U_y \end{pmatrix} \tag{4}$$

These expressions permit to evaluate the total stresses within a poroelastic halfspace. The following constitutive equations consider the two Lamé coefficients λ and μ and the two Biot coefficients M and α. The value σ_f describes the total fluid stresses.

$$
\begin{pmatrix} \sigma_{xx} \\ \sigma_{yy} \\ \tau_{xy} \\ \sigma_f \end{pmatrix} = \begin{bmatrix} \lambda + 2\mu + \alpha^2 M & \lambda + \alpha^2 M & 0 & \alpha M \\ \lambda + \alpha^2 M & \lambda + 2\mu + \alpha^2 M & 0 & \alpha M \\ 0 & 0 & \mu & 0 \\ \alpha M & \alpha M & 0 & M \end{bmatrix} \begin{pmatrix} \varepsilon_{xx} \\ \varepsilon_{yy} \\ \gamma_{xy} \\ \zeta \end{pmatrix} \tag{5}
$$

Symbol	Value	Definition
ρ_s	$2650 \ \mathrm{kg/m^3}$	density, solid matrix
ρ_f	$1000 \ \mathrm{kg/m^3}$	density, water
n^f	0.20	porosity
ρ	$2320 \ \mathrm{kg/m^3}$	density, mixture
η	0.00	loss factor, drained rock
E	$19.333 \cdot 10^9 \ \mathrm{N/m^2}$	E-modulus, drained rock
ν	0.30	Poisson's ratio
K	$18.891 \cdot 10^9 \ \mathrm{N/m^2}$	bulk modulus, mixture
α	0.55	first Biot coefficient
M	$9.11 \cdot 10^9 \ \mathrm{N/m^2}$	second Biot coefficient
k_c	$[10^{-6}; 10^{-2}] \ \mathrm{m/s}$	hydraulic conductivity
a_t	1.0	tortuosity

Table 1: Material parameters for water saturated sandstone [6, 18]

2.2 Description of a poroelastic halfspace with the Wave Based Method

The Wave Based Method (WBM) permits to approximate the displacement fields for the solid skeleton $\mathbf{u}^s$ and the fluid seepage field $\mathbf{U}$ by a sum of weighted wave functions. The following equations refer to displacement fields, which are described by their homogeneous solution. For this, the equations (1) and (2) are approximated by the following WBM approaches $\widehat{\mathbf{u}}_h^s$ and $\widehat{\mathbf{U}}_h$.

$$
\mathbf{u}^s \cong \widehat{\mathbf{u}}_h^s = \sum_{i=1}^{n_{p1}} c_{p1,i} \boldsymbol{\nabla} \Phi_{p1,i} + \sum_{j=1}^{n_{p2}} c_{p2,j} \boldsymbol{\nabla} \Phi_{p2,j} + \sum_{k=1}^{n_s} c_{s,k} \widetilde{\boldsymbol{\nabla}} \Psi_{s,k} \tag{6}
$$

$$
\mathbf{U} \cong \widehat{\mathbf{U}}_h = \sum_{i=1}^{n_{p1}} \gamma_{p1} c_{p1,i} \boldsymbol{\nabla} \Phi_{p1,i} + \sum_{j=1}^{n_{p2}} \gamma_{p2} c_{p2,j} \boldsymbol{\nabla} \Phi_{p2,j} + \sum_{k=1}^{n_s} \gamma_s c_{s,k} \widetilde{\boldsymbol{\nabla}} \Psi_{s,k} \tag{7}
$$

The wave functions $\Phi_{p1,i}$, $\Phi_{p2,j}$ and $\Psi_{s,k}$ are chosen according to [11] and are derived from the underlying analytical solution for an elastodynamic problem, as shown by [8]. These permit to describe the displacement fields of convex domains, by approximating each body wave (P- and S-waves) with a finite number of wave functions. The minimum number of wave functions (n_{p_1}, n_{p_2}, n_s) is derived from the maximum wave number, respectively the highest oscillating wave, used in a WBM approach, which must be larger than the truncated physical wave number of the approximated body wave [7]. This relation is given by the following equation, in which the parameter T denotes a truncation factor chosen by the user. For the simulation results presented in this paper, the value is set to $T = 2$, based on the publications by [8, 11].

$$
k^{\max} \geq T \cdot k, \qquad T \in [1; 6] \tag{8}
$$

In the equations (6) and (7), the unknowns $c_{p_1,i}, c_{p_2,j}$ and $c_{s,k}$ represent the weighting values of the wave functions for a boundary value problem and are derived within a weighted residual Galerkin approach. Figure 1 shows an exemplary boundary value problem, which is divided into two convex subdomains, whose edges are described by different boundary conditions. These consist of Neumann (Γ_σ), coupling ($\Gamma_{(\alpha,\beta)}$), mixed (Γ_{SE}) and absorbing (Γ_Z) boundary conditions, defined according to the publications [14, 19, 20].
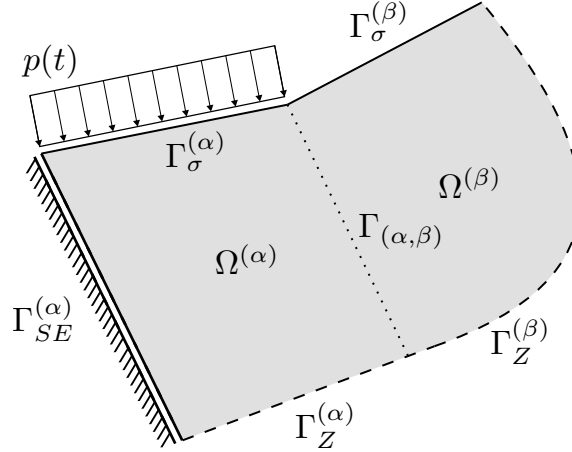
Figure 1: Example for the definition of boundaries

2.3 Description of the displacement fields of a Timoshenko beam

In the following, the displacement field of a beam is divided into its longitudinal $u(s)$ and vertical displacements $y(s)$, which are described separately from each other. The longitudinal and vertical displacements of the beam consist of a homogeneous solution $(u_h(s), y_h(s))$ and a particular solution $(u_p(s), y_p(s))$. The derivation of the longitudinal and vertical displacement fields is for example shown in [21, 22] and applied in [16, 17].

$$u(s) \cong \underbrace{\sum_{r=1}^{2} c_r^{(u)} \Theta_r^{(u)}}_{u_h(s)} + \underbrace{\sum_{m=1}^{n_{(\alpha)}} c_m u_m^{(\alpha)} + \sum_{q=1}^{n_{(\beta)}} c_p u_q^{(\beta)}}_{u_p(s)} \tag{9}$$

$$y(s) \cong \underbrace{\sum_{l=1}^{4} c_l^{(y)} \Theta_l^{(y)}}_{y_h(s)} + \underbrace{\sum_{m=1}^{n_{(\alpha)}} c_m y_m^{(\alpha)} + \sum_{q=1}^{n_{(\beta)}} c_p y_q^{(\beta)}}_{y_p(s)} \tag{10}$$

The homogeneous solution $u_h(s)$ consists of two wave functions $[\Theta^{(u)}]$, whereas $y_h(s)$ is presented by four wave functions $[\Theta^{(y)}]$. These are derived analytically by assessing the underlying dynamic equations for the unloaded case of a longitudinal rod and a Timoshenko beam [15]. The homogeneous solutions depend either on the wave number $k_{(u)}$ (longitudinal rod) or on the two wave numbers $k_{(y,1)}$ and $k_{(y,2)}$ (Timoshenko beam). The values, which are necessary to evaluate these wave numbers, are summarized in Table 2.

$$[\Theta^{(u)}] = [\mathrm{e}^{\mathrm{i}k_{(u)}s}, \mathrm{e}^{-\mathrm{i}k_{(u)}s}], \qquad k_{(u)} = \sqrt{\omega^2 \cdot \rho/E} \tag{11}$$

$$[\Theta^{(y)}] = [e^{ik_{(y,1)}s}, e^{-ik_{(y,1)}s}, e^{ik_{(y,2)}s}, e^{-ik_{(y,2)}s}] \tag{12}$$

$$k_{(y,1)} = \pm\sqrt{\left(-\chi + \sqrt{\chi^2 + 4\varsigma}\right)/2}, \qquad k_{(y,2)} = \pm\sqrt{\left(-\chi - \sqrt{\chi^2 + 4\varsigma}\right)/2}$$

Symbol	Value	Definition
E	$210 \cdot 10^9$ N/m^2	Young's E-modulus
η	0.10	loss factor
ν	0.30	Poisson's ratio
ρ	7850 kg/m^3	density
T	$[0.5; 1.5] \cdot \lambda_r$	length
B	$\{0.10; 0.05\} \cdot T$	width
G	$E/(2 \cdot (1 + \nu))$	shear modulus
A	1 m $\cdot B$	cross section
I	1 m $\cdot B^3/12$	second moment of inertia
κ	$10 \cdot (1 + \nu)/(12 + 11 \cdot \nu)$	shear correction factor
χ	$-\frac{\rho\omega^2}{G\kappa} - \frac{\rho\omega^2}{E}$	–
ς	$-\frac{\rho^2\omega^4}{EG\kappa} + \frac{\rho A\omega^2}{EI}$	–
$\widetilde{A}$	$\frac{1}{EI} - \frac{\rho\omega^2}{EGA\kappa}$	–
$\widetilde{B}$	$\frac{1}{GA\kappa}$	–

Table 2: Parameters for the Timoshenko beam with respect to the Rayleigh wave length λ_r [6]

For the particular solution of the longitudinal and vertical displacement field, it is necessary to evaluate the tangential and normal stresses of the attached WBM domains, as indicated in Figure 2. The difference between the tangential stresses $\sigma_t^{(\alpha)}$ and $\sigma_t^{(\beta)}$ then corresponds to the longitudinal loading q_t, generating longitudinal displacements along the beam. In contrast to this, the normal stresses $\sigma_{n/f}^{(\alpha)}$ and $\sigma_{n/f}^{(\beta)}$ contribute to the normal loading q_n, which causes vertical displacements along the beam. The following particular solutions describe the displacements $[u^{(\diamond)}(s)]$ and $[y^{(\diamond)}(s)]$, with $\diamond \in [\alpha, \beta]$. The stresses $[\sigma_t^{(\diamond)}]$ and $[\sigma_{n/f}^{(\diamond)}]$ depend on the wave functions of the respective domain $\Omega^{(\diamond)}$. The function $\mathrm{H}(s)$ corresponds to the Heaviside step function.

$$[u^{(\diamond)}(s)] = \frac{i}{2EAk_{(u)}} \cdot \int_0^L [\sigma_t^{(\diamond)}(\xi)] \cdot \mathrm{H}(s - \xi) \cdot \left(e^{ik_{(u)}(s-\xi)} - e^{-ik_{(u)}(s-\xi)}\right) \mathrm{d}\xi \tag{13}$$

$$[y^{(\diamond)}(s)] = \frac{i}{2(k_{(y,1)}^2 - k_{(y,2)}^2)} \cdot \int_0^L \frac{\widetilde{A} + k_{(y,1)}^2\widetilde{B}}{k_{(y,1)}} \cdot [\sigma_{n/f}^{(\diamond)}(\xi)] \cdot \mathrm{H}(s-\xi) \cdot \left(e^{ik_{(y,1)}(s-\xi)} - e^{-ik_{(y,1)}(s-\xi)}\right) \ldots$$

$$\ldots - \frac{\widetilde{A} + k_{(y,2)}^2\widetilde{B}}{k_{(y,2)}} \cdot [\sigma_{n/f}^{(\diamond)}(\xi)] \cdot \mathrm{H}(s - \xi) \cdot \left(e^{ik_{(y,2)}(s-\xi)} - e^{-ik_{(y,2)}(s-\xi)}\right) \mathrm{d}\xi \tag{14}$$

For the evaluation of the internal forces of a Timoshenko beam, it is necessary to compute the angular rotation $\varphi(s)$. The homogeneous and particular solution for $\varphi(s)$ are derived from the underlying dynamic equations [15], which is similar to the derivation procedure for $y(s)$. The angle of shear is then defined as follows.

$$\gamma = y' - \varphi \qquad (15)$$
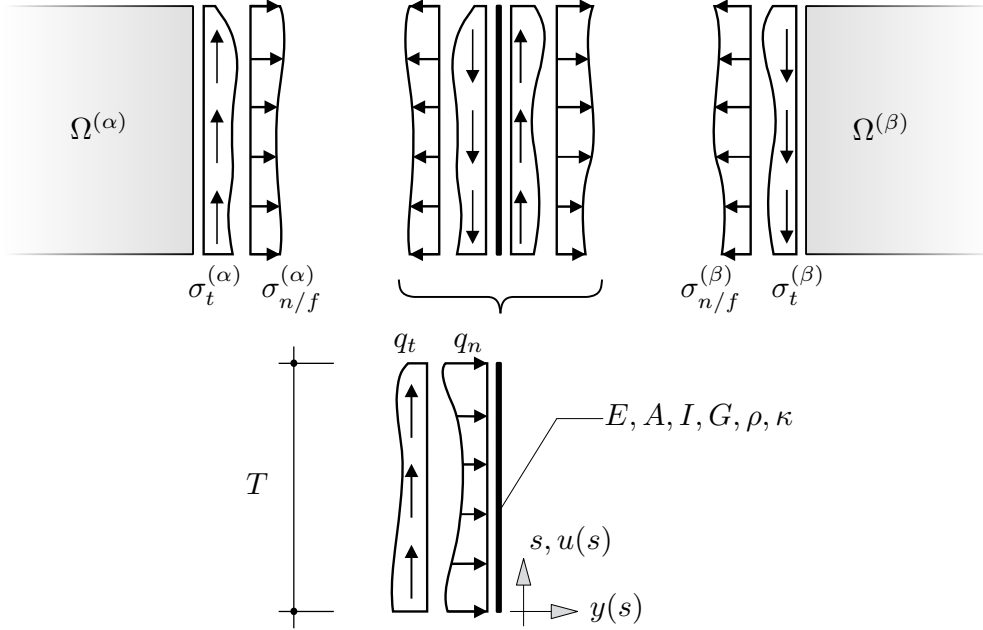
Figure 2: Stresses from coupled WBM domains acting on a beam

2.4 Coupling of the displacement field of a Timoshenko beam to a poroelastic halfspace

The following coupling approach describes the connection of the displacement field of a Timoshenko beam to a poroelastic halfspace, and is based on the coupling procedure between a Kirchhoff plate and an acoustic cavity according to [7]. Therefore, it is necessary to set up compatibility conditions between the normal and tangential displacements of a WBM domain $\Omega^{(\diamond)}$, with $\diamond \in \{\alpha, \beta\}$, and the beam. In the case of a water saturated halfspace, the beam is assumed to be impermeable, so that the fluid flux along the coupled edge of a WBM domain is set to $U_n^{(\diamond)} = 0$. These compatibility conditions are defined for each coupled WBM domain.

$$R^{(\alpha,\text{beam})}(\mathbf{r}) = \begin{cases} R_{u_n}^{(\alpha,\text{beam})}(\mathbf{r}) & = u_n^{(\alpha)} - y = 0 \\ R_{u_t}^{(\alpha,\text{beam})}(\mathbf{r}) & = u_t^{(\alpha)} - u = 0 \\ R_{U_n}^{(\alpha,\text{beam})}(\mathbf{r}) & = U_n^{(\alpha)} = 0 \end{cases} \qquad (16)$$

$$R^{(\beta,\text{beam})}(\mathbf{r}) = \begin{cases} R_{u_n}^{(\beta,\text{beam})}(\mathbf{r}) & = u_n^{(\beta)} + y = 0 \\ R_{u_t}^{(\beta,\text{beam})}(\mathbf{r}) & = u_t^{(\beta)} + u = 0 \\ R_{U_n}^{(\beta,\text{beam})}(\mathbf{r}) & = U_n^{(\beta)} = 0 \end{cases} \qquad (17)$$

In the next step, these compatibility conditions go through a weighted residual Galerkin approach, to set up their contributions to the final system of linear equations. Its unknowns

represent the weighting values for the wave functions of the WBM domains and the weighting values for the homogeneous solution of the longitudinal and vertical displacement field of the beam. The last contributions to the final system of linear equations represent the boundary conditions of the coupled beam in the model. The two ends of the beam are supposed to be free, so that the normal force, the shear force and the moment have to be zero at these points.

$$R^{(\text{beam},\alpha/\beta)}(\mathbf{r}) = \begin{cases} \text{N}(0) & = EA \cdot u'(0) = 0 \\ \text{N}(L) & = EA \cdot u'(L) = 0 \\ \text{Q}(0) & = GA\kappa \cdot \gamma(0) = 0 \\ \text{Q}(L) & = GA\kappa \cdot \gamma(L) = 0 \\ \text{M}(0) & = -EI \cdot \varphi'(0) = 0 \\ \text{M}(L) & = -EI \cdot \varphi'(L) = 0 \end{cases} \tag{18}$$

3 NUMERICAL EXAMPLE

3.1 Model description

Figure 3 depicts a water saturated halfspace, which is excited by a harmonic line loading $p(t) = p_0 \cdot \text{e}^{\text{i}\Omega t}$ with the amplitude $p_0 = 100$ N/m and the excitation frequency $f = 350$ Hz ($\Omega = 2\pi f$). This loading results in a Rayleigh wave length of approximately 5 m, which is evaluated according to the derivations of [6]. The material data for the poroelastic halfspace and the coupled beam are given in Table 1 and Table 2, referring to [6, 18]. The dissipation coefficient ξ is described as a dimensionless value $\xi^* = \xi \cdot T/\sqrt{\mu\rho}$, which is chosen to be $\xi^* = 0.2$ for the following evaluations in order to compare them with the results given by [6]. The dimensionless dissipation coefficient ξ^* and the trench length T become then decisive for the computation of the hydraulic conductivity, which is described within the equation 3.
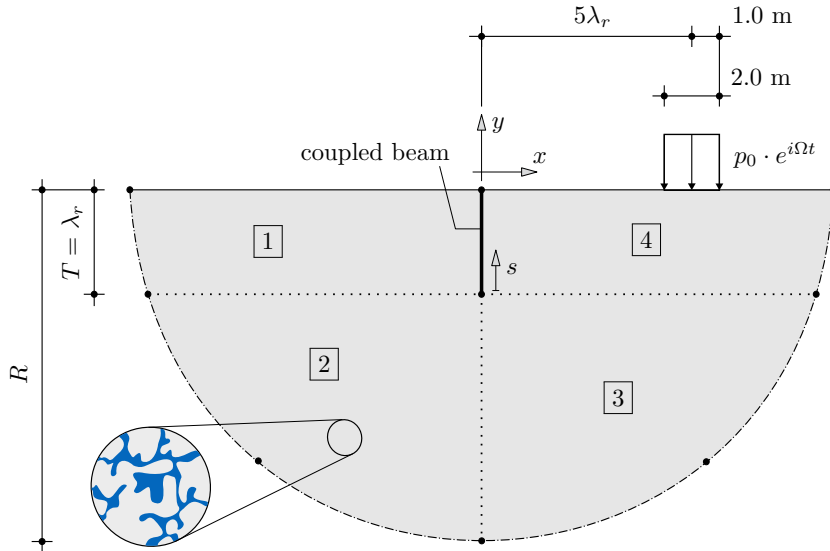
Figure 3: Model description of a beam coupled to a water saturated halfspace

The poroelastic halfspace in Figure 3 is divided into four domains $\boxed{1}$ - $\boxed{4}$, of which each is defined by four nodes. The surface of the halfspace is modeled with Neumann boundary conditions and the circular edges correspond to absorbing boundaries, which transmit incident

wave fronts [14]. The domains $\boxed{1}$ and $\boxed{4}$ are coupled to a beam with the length T and the local s-coordinate system. Dotted lines indicate that two domains are coupled by compatibility and equilibrium equations [20].

Figure 4 illustrates the absolute value for the displacement $|u_y|$ in vertical direction in the vicinity of the coupled beam for $T = \lambda_r$ and $T/B = 10$ ($\lambda_r = 5$ m). The peaks and valleys in front of the barrier indicate that the incoming Rayleigh wave is reflected, as especially the distance between two valleys corresponds to about $\lambda_r/2$. In front of the beam, the absolute value of the vertical displacement goes up to $|u_y| = 3.3 \cdot 10^{-9}$ m along the surface. Behind the trench in its shadow zone, these values decrease and are between $1.0 \cdot 10^{-9}$ m and $1.3 \cdot 10^{-9}$ m. In order to show exemplarily that the defined boundary conditions from equation (18) are fulfilled, Figure 5 depicts the real part of the moment $M(s)$ for the Timoshenko beam. It can be seen, that the moment vanishes at both ends, which fulfills the predefined boundary conditions adequately.
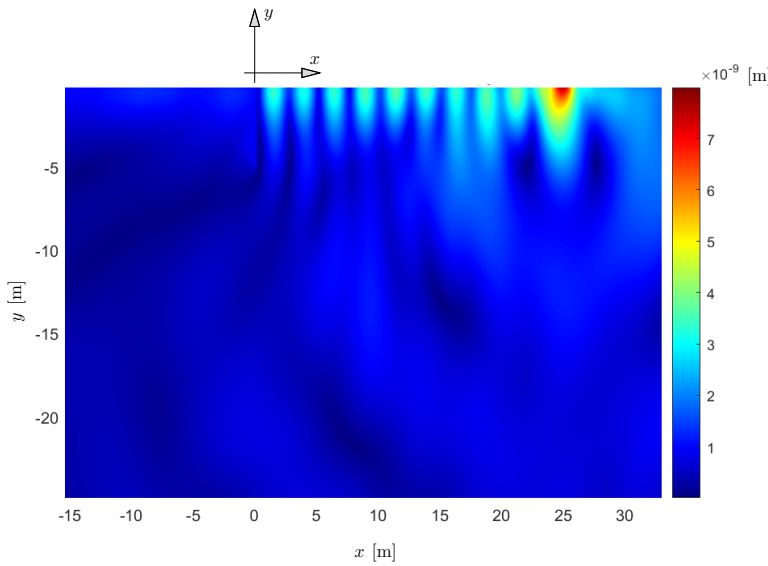
Figure 4: Absolute value of the vertical displacement amplitude $|u_y|$ for the water saturated halfspace coupled to a Timoshenko beam
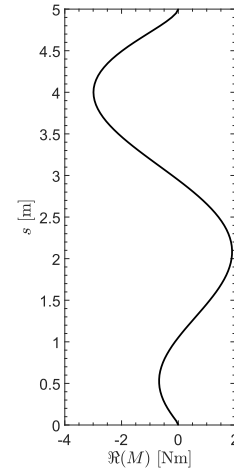
Figure 5: Real part of the moment for the Timoshenko beam

3.2 Convergence of the WBM model

For the presented example, the sum of the square of the residuals for the compatibility conditions between the WBM domains ($\Omega^{(\alpha)}, \Omega^{(\beta)}$) and the coupled beam is evaluated. Two integral expressions are set up, to compute the square of the residuals for the longitudinal and vertical displacements along the beam length T. These residuals are given by the equations (16) and (17). The expression $\widehat{\diamond}$ denotes here a complex conjugate field variable.

$$\|R_u\|_2 = \int_0^T (u_t^{(\diamond)}(s) - u(s)) \cdot (\widehat{u}_t^{(\diamond)}(s) - \widehat{u}(s)) \, \mathrm{d}s, \quad \text{with } \diamond \in \{\alpha, \beta\} \tag{19}$$

$$\|R_y\|_2 = \int_0^T (u_n^{(\diamond)}(s) - y(s)) \cdot (\widehat{u}_n^{(\diamond)}(s) - \widehat{y}(s)) \, \mathrm{d}s, \quad \text{with } \diamond \in \{\alpha, \beta\} \tag{20}$$

These residuals are normalized by the square of the maximum amplitude of the longitudinal displacement ($|u_{\max}|^2$), or respectively the maximum vertical displacement ($|y_{\max}|^2$), of the beam. These values are computed for several sets of wave functions and plotted in Figure 6 and Figure 7. In these figures, the value n_{DOF} denotes the total number of unknowns, respectively the number of degrees of freedom (DOF). Both figures indicate, that the sum of the squared residuals decreases steadily for a higher number of wave functions. However, for $4000 < n_{\mathrm{DOF}} < 6000$, this value remains between 10^{-5} and 10^{-4} without changing significantly. For $1000 < n_{\mathrm{DOF}} < 2000$, a substantial drop is observed in both figures. This indicates, that the generated wave numbers for the wave functions of the WBM domains are lower than the physical wave numbers for the body waves of the poroelastic halfspace and the Timoshenko beam. This violates the condition defined in equation (8), revealing a strong mismatch between the coupled displacement fields of the beam and the attached domains.
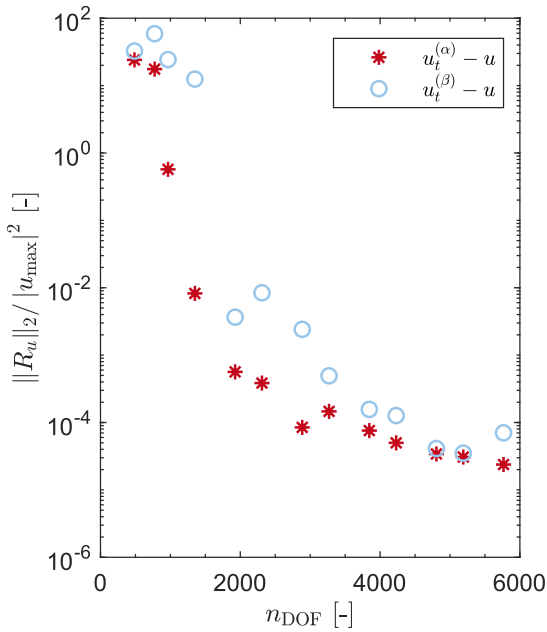
Figure 6: $\|R\|_2$ for the longitudinal displacements along the coupled beam
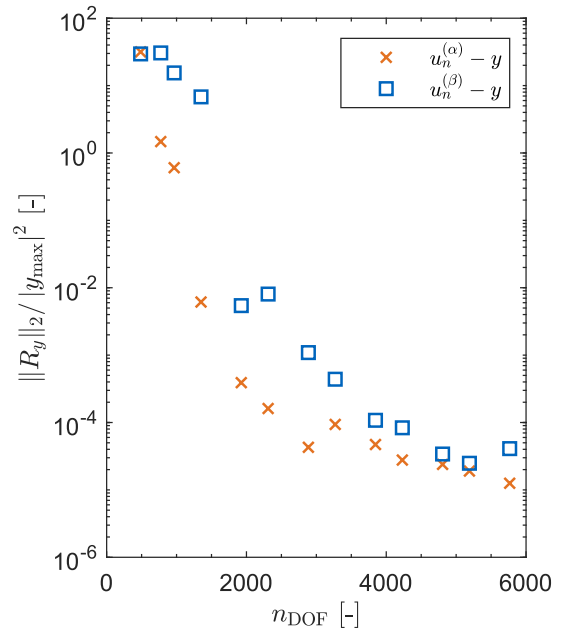
Figure 7: $\|R\|_2$ for the vertical displacements along the coupled beam

3.3 Comparison with reference data

To compare the introduced example in Figure 3 with data from literature [6], the average vertical displacement amplitude reduction ratio $\overline{A}_y$ is calculated.

$$\overline{A}_y = \frac{1}{10\lambda_r} \int\limits_0^{-10\lambda_r} \frac{|u_{y,\mathrm{beam}}(x, y = 0)|}{|u_{y,\mathrm{ref}}(x, y = 0)|} \, \mathrm{d}x \tag{21}$$

$\overline{A}_y$ corresponds to the mean value of the ratio between the absolute displacement amplitudes $|u_{y,\mathrm{beam}}|$ and $|u_{y,\mathrm{ref}}|$. The value $|u_{y,\mathrm{beam}}|$ stands for displacements with an installed beam, whereas $|u_{y,\mathrm{ref}}|$ refers to the displacement field without a wave barrier. In the following, $\overline{A}_y$ is evaluated along the surface of the halfspace in the shadow zone of the beam, respectively for $x \in [0; -10\lambda_r]$ and $y = 0$.

Figure 8 depicts results for $\overline{A}_y$ in dependency of the trench length $T/\lambda_r \in [0.5; 1.5]$ and the trench widths B, which is chosen as $T/B \in \{10; 20\}$. For $T/\lambda_r \leq 1.3$, the average reduction ratio $\overline{A}_y$ with the WBM model lies under the results by [6], in which a BEM-FEM approach is used. The maximum difference is 0.051 for $T/B = 10$ and 0.029 for $T/B = 20$. The best compliance is reached for $T/\lambda_r > 1.3$ with differences of 0.008 ($T/B = 10$) and 0.004 ($T/B = 20$). The presented data indicates that the WBM model predicts mostly lower values for $\overline{A}_y$ than the BEM-FEM approach. This corresponds to a slightly higher mitigation efficiency of the beam according to the WBM model. However, these differences are still in an acceptable range.
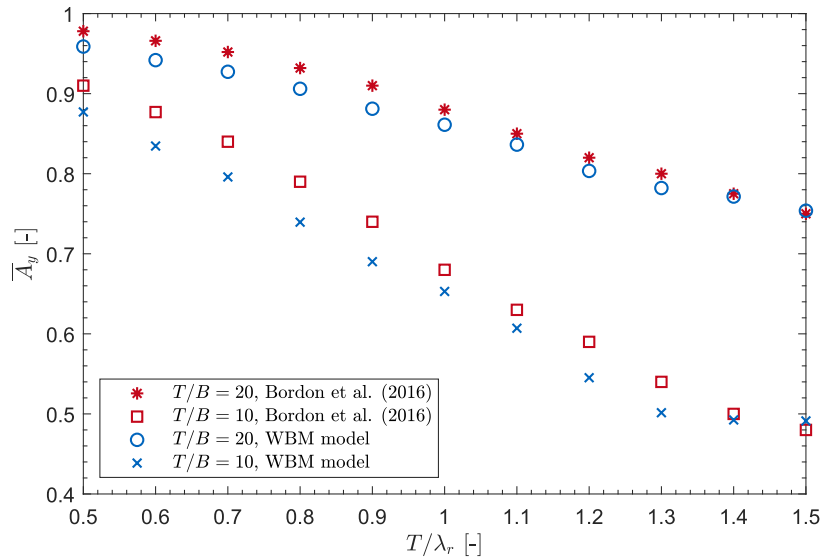
Figure 8: Comparison of $\overline{A}_y$ in dependency of the trench length L and the width B, computed with the WBM model and a BEM-FEM approach [6]

3.4 CONCLUSION

In this paper, the Wave Based Method (WBM) is extended by Biot's theory for low frequencies [12, 13] and coupled to the analytical solution of the Timoshenko beam [15, 16]. This coupling approach is based on [7], in which a Kirchhoff plate is connected to an acoustic cavity. The presented coupling approach permits to model a water saturated halfspace with a simple wall, which is installed as a wave barrier against an incoming Rayleigh wave. It is shown that the residuals of the compatibility conditions between the beam and the attached halfspace reduce significantly and also converge for an increasing number of wave functions. For a total number of unknowns between 1000 and 2000 considerable drops are observed for the squared residuals of the coupled displacement fields. The reason for this is, that the wave numbers of the wave function sets of the WBM domains become lower than the wave numbers of the approximated body waves within the halfspace. Moreover, the average vertical displacement amplitude reduction ratio is evaluated for different trench dimensions and compared with results from the BEM-FEM model presented in [6]. The simulation results with the WBM approach reveal an adequate accordance with the data from the BEM-FEM model.

REFERENCES

[1] W. Haupt, Isolation of vibrations by concrete core walls. *Proceedings of the 9th International Conference on Soil Mechanics and Foundation Engineering*, Tokyo, Japan, 1977.

[2] D. Beskos, B. Dasgupta, I. Vardoulakis, Vibration isolation using open or filled trenches. *Computational Mechanics*, **1**(1), 43-63, 1986.

[3] J. Freisinger, G. Müller, Coupled ITM-FEM approach for the assessment of the mitigation efficiency of finite and infinite open trenches and infilled barriers. *XI International Conference on Structural Dynamics (EURODYN 2020)*, Athens, Greece, November 23-26, 2020.

[4] A.E. Moghadam, R. Rafiee-Dehkharghani, Ground-borne vibration screening in layered dry and saturated grounds using optimal inclined wave barriers. *Soil Dynamics and Earthquake Engineering*, **162**, 2022.

[5] J.P. Li, X.L. Zhang, S.J. Feng, Z.L. Chen, Y.C. Li, Numerical Investigation of ground-borne vibration mitigation by infilled trenches in a poroelastic half-space considering the moving water table. *International Journal of Geomechanisc*, **21**(10), 2021.

[6] J.D.R. Bordón, J.J. Aznárez, O. Maeso, Two-dimensional numerical approach for the vibration isolation analysis of thin walled wave barriers in poroelastic soils. *Computers and Geotechnics*, **71**, 168-179, 2016.

[7] W. Desmet, *A wave based prediction technique for coupled vibro-acoustic analysis, PhD. thesis 98D12*. Faculteit Toegepaste Wetenschappen, Katholieke Universiteit Leuven, 1998.

[8] C. Vanmaele, *Development of a wave based prediction technique for the efficient analysis of low- and mid-frequency structural vibrations, PhD. thesis 2007D11*. Faculty of Engineering, Katholieke Universiteit Leuven, 2007.

[9] B. Van Hal, *Automation and performance optimization of the wave based method for interior structural-acoustic problems, PhD Thesis*. Faculteit Toegepaste Wetenschappen, Katholieke Universiteit Leuven, 2004.

[10] B. Pluymers, *Wave based modelling methods for steady-state vibroacoustics, PhD thesis 2006D04*. Faculty of Engineering, Katholieke Universiteit Leuven, 2006.

[11] E. Deckers, *A wave based approach for steady-state Biot models of poroelastic materials, PhD. thesis 2012D12*. Faculty of Engineering, Katholieke Universiteit Leuven, 2012.

[12] M.A. Biot, Theory of propagation of elastic waves in a fluid-saturated porous solid. I. Low-frequency range. *Journal of the Acoustical Society of America*, **28**(2), 168-78, 1956.

[13] M.A. Biot, Mechanics of deformation and acoustic propagation in porous media. *Journal of Applied Physics*, **33**(4), 1482-98, 1962.

[14] G. Degrande, *A spectral and finite element method for wave propagation in dry and saturated poroelastic media, PhD Thesis*. Katholieke Universiteit Leuven, 1992.

[15] S.P. Timoshenko, LXVI. On the correction for shear of the differential equation for transverse vibrations of prismatic bars. *The London, Edinburgh, and Dublin Philosophical Magazine and Journal of Science*, **41**, 744-746, 1921.

[16] G.G.G. Lueschen, L.A. Bergman, D.M. McFarland, Green's functions for uniform Timoshenko beams. *Journal of Sound and Vibration*, **194**(1), 93-102, 1996.

[17] C.M. Wang, K.Y. Lam, X.Q. He, Exact solutions for Timoshenko beams on elastic foundations using Green's functions. *Mechanics of Structures and Machines*, **26**(1), 101-113, 1998.

[18] C.H. Lin, V.W. Lee, M.D. Trifunac, The reflection of plane waves in a poroelastic halfspace saturated with inviscid fluid. *Soil Dynamics and Earthquake Engineering*, **25**(3), 205-223, 2005.

[19] P. Debergue, R. Panneton, N. Atalla, Boundary conditions for the weak formulation of the mixed (u,p) poroelasticity problem. *Journal of the Acoustical Society of America*, **106**(5), 2383–2390, 1999.

[20] J.F. Allard, N. Atalla, *Propagation of sound in porous media: modelling sound absorbing materials*. JohnWiley & Sons, 2009.

[21] J.F. Doyle, *Wave propagation in structures, 2nd Edition*. Springer-Verlag New York, 1997.

[22] M.C. Junger, D. Feit, *Sound, structures and their interaction, 2nd Edition*. The MIT Press, 1986.